© 2019. Published by The Company of Biologists Ltd | Journal of Experimental Biology (2019) 222, jeb212464. doi:10.1242/jeb.212464

RESEARCH ARTICLE

Thrust generation during steady swimming and acceleration from rest in anguilliform swimmers

Kevin T. Du Clos[1,‡], John O. Dabiri[2], John H. Costello[3], Sean P. Colin[4], Jennifer R. Morgan[5], Stephanie M. Fogerson[5,*] and Brad J. Gemmell[1]

ABSTRACT

Escape swimming is a crucial behavior by which undulatory swimmers evade potential threats. The hydrodynamics of escape swimming have not been well studied, particularly for anguilliform swimmers, such as the sea lamprey *Petromyzon marinus*. For this study, we compared the kinematics and hydrodynamics of larval sea lampreys with those of lampreys accelerating from rest during escape swimming. We used experimentally derived velocity fields to calculate pressure fields and distributions of thrust and drag along the body. Lampreys initiated acceleration from rest with the formation of a high-amplitude body bend at approximately one-quarter body length posterior to the head. This deep body bend produced two high-pressure regions from which the majority of thrust for acceleration was derived. In contrast, steady swimming was characterized by shallower body bends and negative-pressure-derived thrust, which was strongest near the tail. The distinct mechanisms used for steady swimming and acceleration from rest may reflect the differing demands of the two behaviors. High-pressure-based mechanisms, such as the one used for acceleration from rest, could also be important for low-speed maneuvering during which drag-based turning mechanisms are less effective. The design of swimming robots may benefit from the incorporation of such insights from unsteady swimming.

KEY WORDS: *Petromyzon marinus*, Lamprey, Undulatory, Thrust, Drag

INTRODUCTION

Spatially and temporally resolved flow data, such as those obtained from particle image velocimetry (PIV), have greatly advanced our understanding of fish swimming (as reviewed in Lauder and Tytell, 2005; Lauder, 2015), particularly when combined with kinematic data, which have been available for much longer (e.g. Gray, 1933). Recently developed techniques go a step further, using velocity fields derived from PIV or other experimental techniques to calculate pressure fields with high spatial and temporal resolution (e.g. Noca et al., 1997; Gurka et al., 1999; Noca et al., 1999; van Oudheusden et al., 2007; Dabiri et al., 2014). Pressure fields are valuable because they can be used to calculate the magnitude and distribution of forces acting on a swimming fish, but high-resolution pressure data have traditionally been difficult to obtain experimentally, particularly for unsteady flows.

Here, we used a pressure calculation method first presented in Dabiri et al. (2014). The technique has previously been used to calculate pressure fields and drag and thrust forces associated with steady swimming in larval sea lampreys, *Petromyzon marinus* (Dabiri et al., 2014; Gemmell et al., 2015a, 2016). In this study, we extend these results by comparing the kinematics and hydrodynamics of steadily swimming larval lampreys with those of lampreys accelerating from rest.

While 3D velocimetry methods have proven effective for studying swimming hydrodynamics away from the body, such as in the wake (e.g. Flammang et al., 2011), we chose to use 2D PIV for this study for its ability to better capture velocities close to moving surfaces (Gemmell et al., 2014, 2015b). This study was focused on near-body flows, so it was particularly important to accurately measure velocities adjacent to the body to produce pressure fields from which we could calculate forces acting on the body. These experimental data will be important for validating future computational models of undulatory swimmers. While 2D PIV cannot account for out-of-plane velocity, previous validations of this method have shown that it generally performs well with planar data when in-plane velocities dominate thrust generation, as they do for lampreys (Dabiri et al., 2014; Lucas et al., 2017). For a 3D computational fluid dynamics (CFD) model of a swimming lamprey, pressures calculated from planar data extracted from the model agreed well with pressures taken directly from the model (Dabiri et al., 2014). Additionally, a series of experiments with flapping foils that considered 3D effects showed that forces derived from planar PIV data and measurements from force transducers generally agreed (Lucas et al., 2017). When there were differences, the pressure calculation tended to underestimate forces (Lucas et al., 2017).

The anguilliform swimming mode is characterized by undulations of gradually increasing amplitude along the length of the swimmer (Gray, 1933; Gillis, 1996; Lauder and Tytell, 2005). Kinematics suggest that the body (excluding the tail) likely plays a larger role in generating thrust in anguilliform swimming than it does in other swimming modes that are characterized by larger increases in body wave amplitude near the tail (e.g. carangiform swimming). However, previous studies of anguilliform swimming have disagreed about the extent to which the body contributes to thrust and the mechanisms by which it does so (Lighthill, 1971; Carling et al., 1998; Videler et al., 1999; Müller et al., 2001; Tytell and Lauder, 2004; Chen et al., 2011; Gemmell et al., 2016). Many studies of swimming hydrodynamics have focused on properties of vortices shed in the wake of swimming fish (Linden and Turner, 2004; Müller et al., 1997, 2001, 2008; Tytell and Lauder, 2004).

[1]Department of Integrative Biology, University of South Florida, Tampa, FL 33620, USA. [2]Departments of Civil & Environmental Engineering and Mechanical Engineering, School of Engineering, Stanford University, Stanford, CA 94305, USA. [3]Biology Department, Providence College, Providence, RI 02918, USA. [4]Marine Biology and Environmental Science, Roger Williams University, Bristol, RI 02809, USA. [5]Marine Biological Laboratory, Woods Hole, MA 02543, USA.
*Present address: Biology Department, Duke University, Durham, NC 27708, USA.

‡Author for correspondence (duclos@usf.edu)

K.T.D., 0000-0002-3017-7777; J.H.C., 0000-0002-6967-3145

Received 15 August 2019; Accepted 22 October 2019

Journal of Experimental Biology (2019) 222, jeb212464. doi:10.1242/jeb.212464

This approach has provided many insights into swimming mechanics, but it does not provide details on how and where thrust is generated along a fish's body because the effects of thrust and drag cannot be separated in the wake (Schultz and Webb, 2002; Tytell, 2007). In this study, we used pressure data to calculate forces produced along the body, allowing us to determine how different sections of the body contribute to thrust and drag and whether these forces derive primarily from positive or negative pressure.

Escape swimming has been studied from the perspective of kinematics (reviewed in Gazzola et al., 2012; Wakeling, 2005; Domenici and Blake, 1997; Domenici and Hale, 2019), neurobiology (reviewed in Eaton et al., 2001) and to a lesser extent hydrodynamics (e.g. Tytell and Lauder, 2008), but is not well studied in anguilliform swimmers. A few studies have examined escape swimming in larval zebrafish (e.g. Li et al., 2014; Nair et al., 2015), and one study has examined accelerating swimming, though not escape swimming, in eels (Tytell, 2004). Steady swimming behaviors are likely to be optimized for low energy consumption, particularly for *P. marinus*, which perform upstream migrations of several hundred kilometers (Beamish, 1980), whereas for escape swimming, energy consumption is less important than successfully evading a predator. Here, we compare the kinematics and hydrodynamics of steady swimming with those of accelerating escape swimming and present force calculations for each behavior.

MATERIALS AND METHODS

Late larval stage sea lampreys (*P. marinus* Linnaeus 1758) were recorded – either swimming steadily or accelerating from rest – at 1000 frames s^{-1} using a FASTCAM 1024 or FASTCAM Mini WX 100 high-speed camera (Photron, Tokyo, Japan). Filming methods were similar to those described in Gemmell et al. (2015a, 2016). Animals were filmed in one of two acrylic tanks (1.4×0.3 m or 0.5×0.5 m, length×width) filled to 5 cm depth with seawater seeded with 10 µm hollow glass spheres (Potter Industries, Malvern, PA, USA).

The code used to calculate the pressure field from the velocity field can be affected by any out-of-plane flow induced by the presence of the walls (Lucas et al., 2017); as the laser sheet plane is oriented horizontally, the side walls could potentially create out-of-plane flow that could compromise the pressure calculations. Animals were thus filmed far from the tank side walls to minimize lateral wall effects.

The animals tended to swim near the bottom of the tank, so they were filmed there in order to capture their natural swimming behavior. Ground effects may thus have affected swimming performance and hydrodynamics. However, ground effects have been shown to be much more important for flatfish than for fish that direct thrust forces primarily perpendicular to the bottom (Webb, 2002), such as lampreys, and the bottom wall actually suppresses out-of-plane motion, reinforcing the in-plane flow assumption of the pressure calculations. Hence, ground effects should not compromise the pressure calculations. A similar conclusion was examined in the validation study of Lucas et al. (2017). Recent work has shown that ground effects are not limited to accelerating swimming but are present in steady swimming as well (Kurt et al., 2019), suggesting that the presence of ground effects should not bias comparisons between the two swimming modes. Furthermore, using only sequences in which the animal remained in the laser sheet minimized possible ground effect discrepancies between sequences and treatments by ensuring that animals were filmed at the same height above the bottom (~0.1 body lengths, bl; see below) for all sequences.

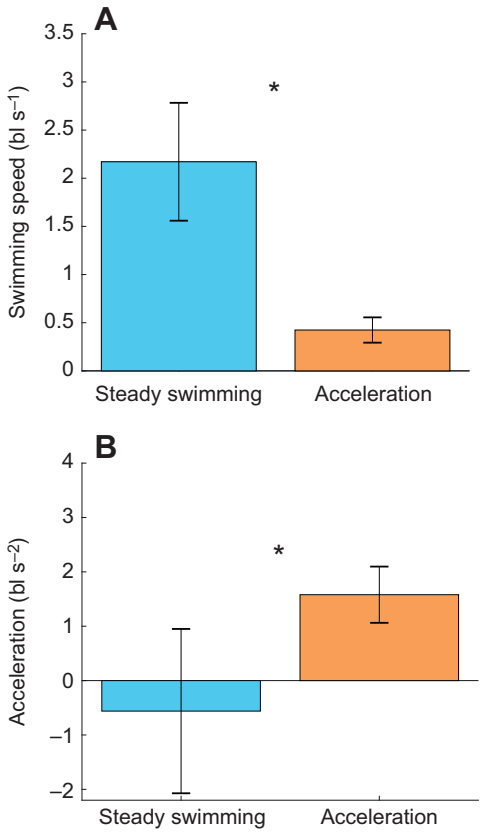

Fig. 1. Swimming speed and acceleration. Means and standard deviations of (A) mean swimming speed and (B) mean acceleration for a half-cycle of steady swimming (n=8) or acceleration from rest (n=8) averaged over one half-cycle of swimming. bl, body length. Asterisks indicate significant differences.

Illumination was provided by two continuous-wave 532 nm, 600 mW lasers mounted at the same height on opposite sides of the tank and focused and spread into overlapping light sheets, eliminating most of the shadows cast by the swimming animal. Juvenile sea lampreys are blind (Wald, 1957) and did not appear to change behavior in response to the laser sheet. Acceleration was induced by gently touching the lamprey on the tip of the tail with a glass stirring rod. All procedures were approved by the Institutional Animal Care and Use Committee at the Marine Biological Laboratory and the University of South Florida and were in accordance with standards set by the National Institutes of Health (NIH).

Videos of eight individuals accelerating from rest were recorded, with at least five videos recorded per animal. Obtaining sequences of acceleration from rest in which the entire animal remained centered in the laser sheet over the entire acceleration period was challenging, so only one sequence of each animal was selected for analysis. Sequences were chosen based on how consistently the animal swam within the laser sheet, and on video quality (e.g. high contrast, minimal reflections). One sequence each of eight steadily swimming lampreys was selected for comparison. Because our goal was to compare acceleration from rest with steady swimming, the steady swimming sequences with the lowest instantaneous acceleration were selected.

Velocity fields were calculated using PIV performed with the DaVis 8.3 software package (LaVision, Göttingen, Germany). Every fifth frame was used for analysis, yielding a separation between frames (dt) of 5 ms. Calculations were performed using

Journal of Experimental Biology (2019) 222, jeb212464. doi:10.1242/jeb.212464

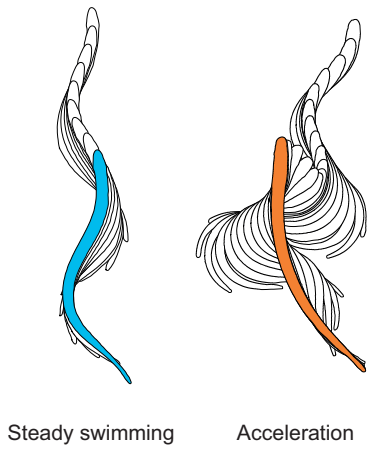

Fig. 2. Body outlines for a half-cycle of steady swimming and a half-cycle of acceleration from rest. The first outline of each sequence is filled.

three passes each with two sets of decreasing interrogation window size, yielding 128×128 vectors per frame.

Additional analyses on PIV-derived velocity fields were performed using MATLAB (MathWorks, Natick, MA, USA). Pressure fields were calculated using the queen 2.0 pressure field calculation package for MATLAB (available at http://dabirilab.com/software; Dabiri et al., 2014). Briefly, pressure gradient terms were first calculated from the velocity fields for two subsequent frames, based on the incompressible Navier–Stokes equations. Pressure at each grid point was then calculated by integrating pressure gradients along eight paths and taking the median result.

Pressure fields were then used to calculate thrust and drag forces per height (because PIV data were 2D) on 60 segments spaced evenly around the body by multiplying the pressure along a segment by the length of the segment and the unit vector in the swimming direction, where thrust forces are positive and drag forces are negative (see Gemmell et al., 2016). Forces were classified as either 'pull' or 'push' forces according to whether they were derived from negative or positive pressure (relative to ambient).

Swimming speed was calculated using the same frames used for PIV analysis, based on the derivative of a piecewise cubic spline fit to centroid displacement over time. Mean and maximum acceleration were calculated from the time derivative of swimming speed. Further kinematic parameters were calculated from centerlines extracted from video sequences using MATLAB. Kinematic parameters were normalized to body length (bl), which was taken to be the mean of centerline length.

All statistical tests were performed using MATLAB. In many cases, data could not be transformed to meet the assumption of normality required for a *t*-test. Non-parametric Mann–Whitney *U*-tests were thus used to test for significant differences between steady and accelerating swimming in kinematic and force parameters. Differences were considered significant if *P*-values were less than α=0.05. Parameters are reported as means±s.d.

RESULTS

Kinematics

Sequences of acceleration from rest (n=8, bl=134.3±8.9 mm) had significantly higher mean acceleration (1.58±0.48 bl s^{-2}, P<0.001) and lower mean swimming speed (0.42±0.12 bl s^{-1}) than steady swimming sequences (P<0.001; Fig. 1). Mean acceleration for steady swimming sequences (n=8, bl=120.5±7.4 mm) was negative (−0.56±1.41 bl s^{-2}), and mean swimming speed was approximately 5 times as fast as for accelerating cases (2.17 ±0.57 bl s^{-1}, P<0.001). The differences in acceleration and swimming speed provided a check on our video selection criteria, assuring us that the two sets of videos contained distinct swimming behaviors.

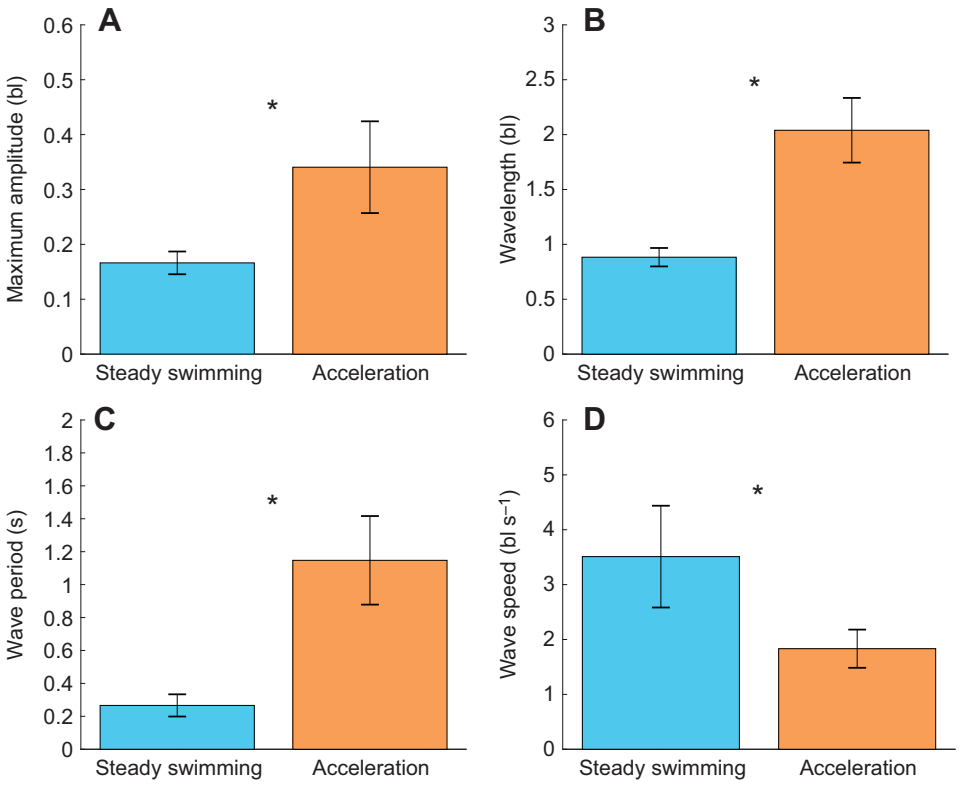

Fig. 3. Kinematics parameters. Means and standard deviations of kinematic parameters averaged over one half-cycle of steady swimming (n=8) or acceleration from rest (n=8): (A) maximum amplitude, (B) wavelength, (C) wave period and (D) body wave speed. Asterisks indicate significant differences.

Journal of Experimental Biology (2019) 222, jeb212464. doi:10.1242/jeb.212464

The kinematics of acceleration differed visibly from those of steady swimming (Fig. 2). Steadily swimming lampreys produced a smooth body wave that moved from head to tail, with amplitude increasing gradually along the length of the body and a nearly constant wave speed.

Accelerating lampreys had deeper body bends than steadily swimming lampreys, with a maximum amplitude that was twice as large (P<0.001; Fig. 3A) and higher amplitudes along the entire length of the body. These body bends often started not at the head but approximately one-quarter body length posterior to the head.

Mean wave period was more than 4 times as long for acceleration (1.15±0.25 s) as for steady swimming (0.27±0.06 s, P<0.001; Fig. 3C). While wavelength was also slightly longer for accelerating than for steady swimming (P<0.001; Fig. 3B), body wave speed was much slower for accelerating (3.51±0.87 bl s^{-1}) than for steady swimming (1.83±0.33 bl s^{-1}, P<0.001; Fig. 3D).

Pressure and forces

We calculated forces acting on the body surface, differentiating between ‘pull’ and ‘push’ forces due to negative or positive pressure

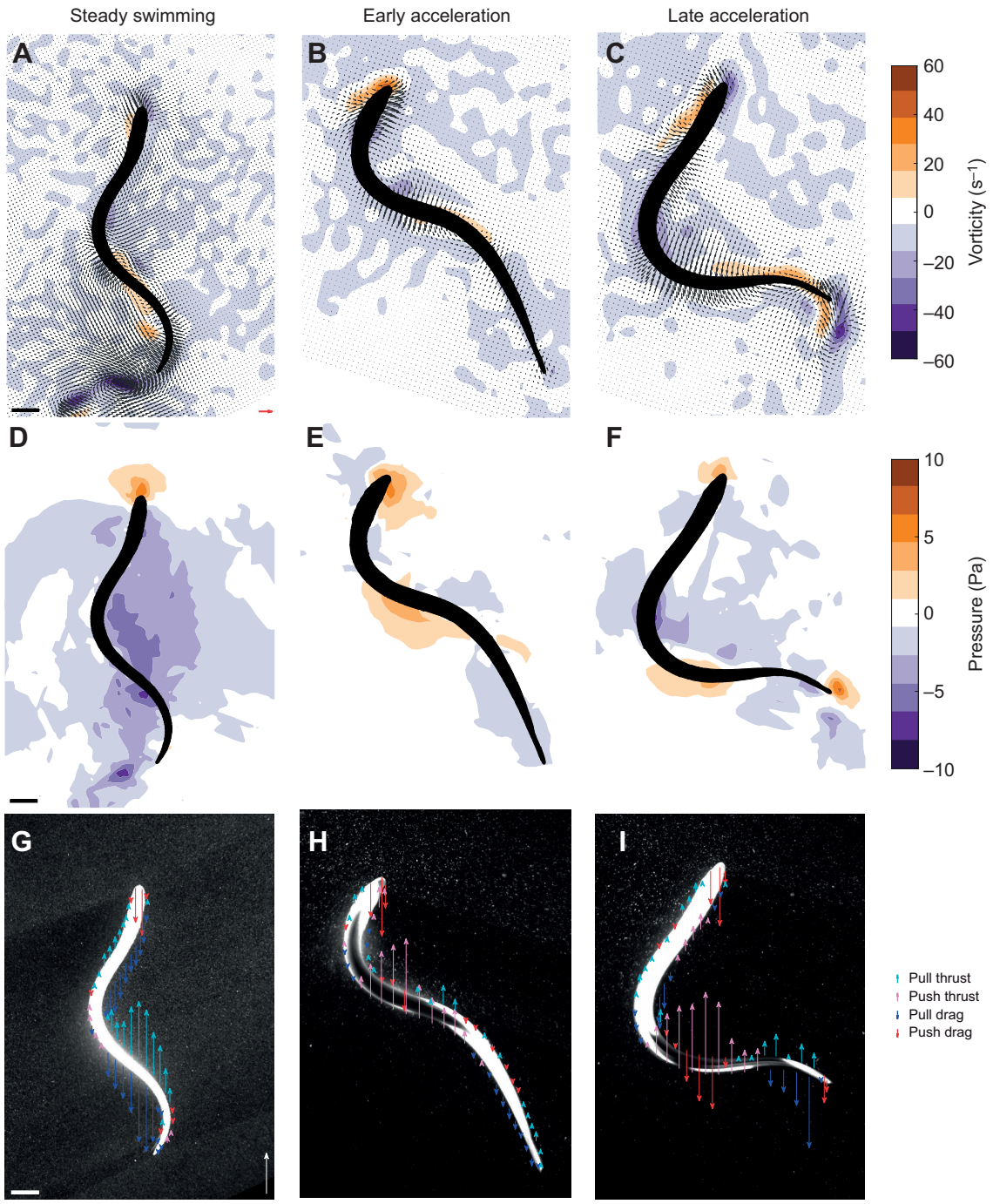

Fig. 4. Vorticity, pressure and force components. Selected frames during steady swimming and early and late phases of acceleration from rest. (A–C) Vorticity fields with velocity vectors. The red scale arrow indicates 100 mm s^{-1}. (D–F) Pressure fields. (G–I) Thrust and drag component vectors. The white scale arrow indicates 0.1 mN cm^{-1}. The scale bars indicate 10 mm for all frames.

Journal of Experimental Biology (2019) 222, jeb212464. doi:10.1242/jeb.212464

(relative to ambient) and between thrust forces acting in the direction of swimming and drag forces acting in the opposite direction (Fig. 4).

Net thrust (thrust minus drag forces) was significantly higher for accelerating (0.20±0.11 mN cm^{-1}) than for steady swimming (−0.05±0.18 mN cm^{-1}, P=0.02; Fig. 5B) as expected, providing an additional check on our video selection criteria. For steady swimming, net thrust forces oscillated around zero, with peaks in net force preceding periods of minor acceleration and troughs in net force preceding periods of minor deceleration (Fig. 6A). By contrast, for the accelerating sequences, net force was more often positive than negative until near the end of the sequence following the initial period of acceleration from rest (Fig. 6B).

For steady swimming sequences, pressure fields were dominated by strong negative pressure along the body associated with body bends (Fig. 4D), which corresponded with strong pull forces (Fig. 4G). Mean pull thrust was nearly 6 times as strong as push thrust for steady swimming, with push thrust accounting for 19 ±21% of total thrust (P<0.001; Fig. 5A,C). For accelerating swimming, by contrast, push thrust was more than twice as strong as pull thrust, accounting for 69±5% of total thrust (P=0.005; Fig. 5A,C). Drag forces followed trends similar to those for thrust forces, with significantly stronger pull drag for steady swimming (P<0.001) and significantly stronger push drag for accelerating swimming (P<0.001).

Distribution of forces along the body

To compare the distribution of forces along the body for steady swimming and acceleration from rest, we divided the body into 12 segments of equal length and for each segment calculated force components averaged over time and treatment (Fig. 7A,B). We also calculated the percentage thrust contributions of the anterior, medial and posterior thirds of the body.

For steady swimming, thrust was due mainly to negative pressure and gradually increased from anterior to posterior, with the anterior, medial and posterior thirds of the body contributing 17.5%, 32.8% and 49.7% of total thrust (Figs 7A, 4G). Net thrust was highest at the posterior third of the body where there was a slight push thrust in addition to a stronger pull thrust. Pull thrust was stronger than push thrust along most of the body.

For the accelerating sequences, the anterior, medial and posterior thirds of the body contributed 22.4%, 35.0% and 42.6% of total thrust. As for steady swimming, the strongest net thrust was at the posterior third of the body. By contrast with steady swimming, net thrust was positive along most of the length of the body for accelerating swimming (Figs 7B, 4G,H). Push thrust dominated over pull thrust along most of the body.

Early versus late acceleration

To examine acceleration in more detail, we calculated the distribution of force components as described above but for the first and second halves (early and late) of the acceleration half-cycle (Fig. 7C,D).

In early acceleration, as a lamprey pulled its head posteriorly toward the body, two high-pressure regions developed: one at the head on the concave side of the initial body bend and one posterior to the bend on the convex side (Fig. 4E,H). The body bend formed at the anterior was often accompanied by a second body bend that formed at approximately the midpoint of the body (not shown). During this time, the strongest thrust was due to positive pressures at the medial third of the body (Fig. 7C). The anterior, medial and posterior thirds of the body contributed 29.8%, 44.8% and 25.4% of thrust. The strong push forces associated with these high-pressure regions were accompanied by weaker contralateral pull forces, which grew as the bend moved toward the tail.

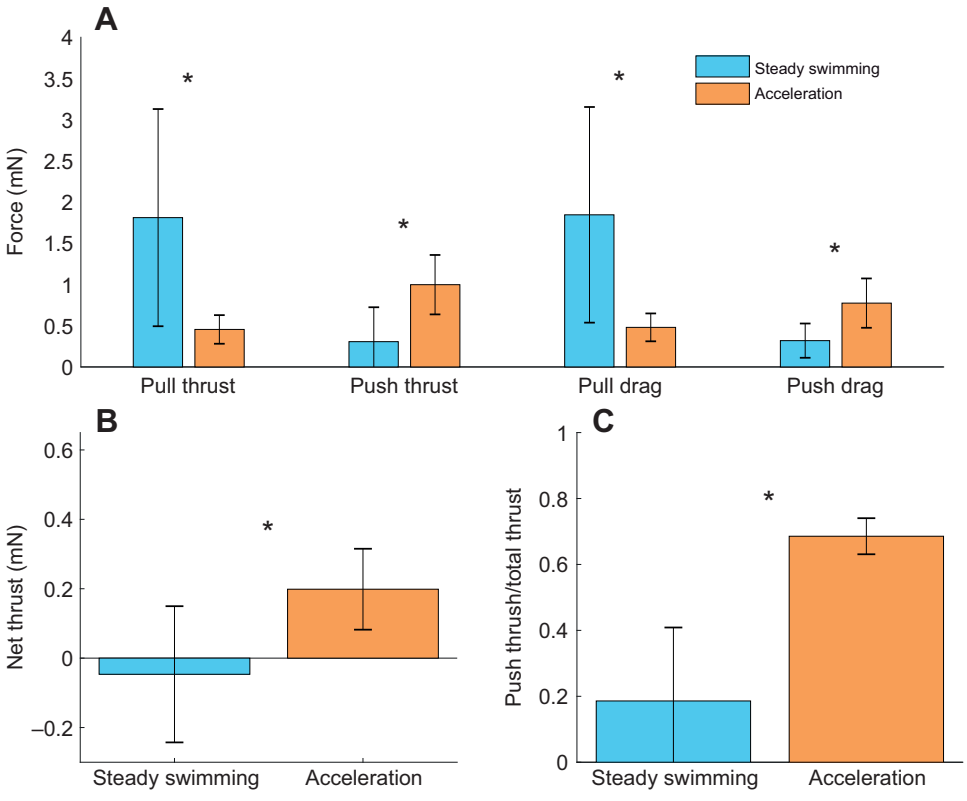

Fig. 5. Force components. Means and standard deviations of (A) force components, (B) net thrust and (C) thrust due to positive pressure (push thrust) divided by total thrust, averaged over one half-cycle of steady swimming (n=8) or acceleration from rest (n=8). Asterisks indicate significant differences.

Journal of Experimental Biology (2019) 222, jeb212464. doi:10.1242/jeb.212464

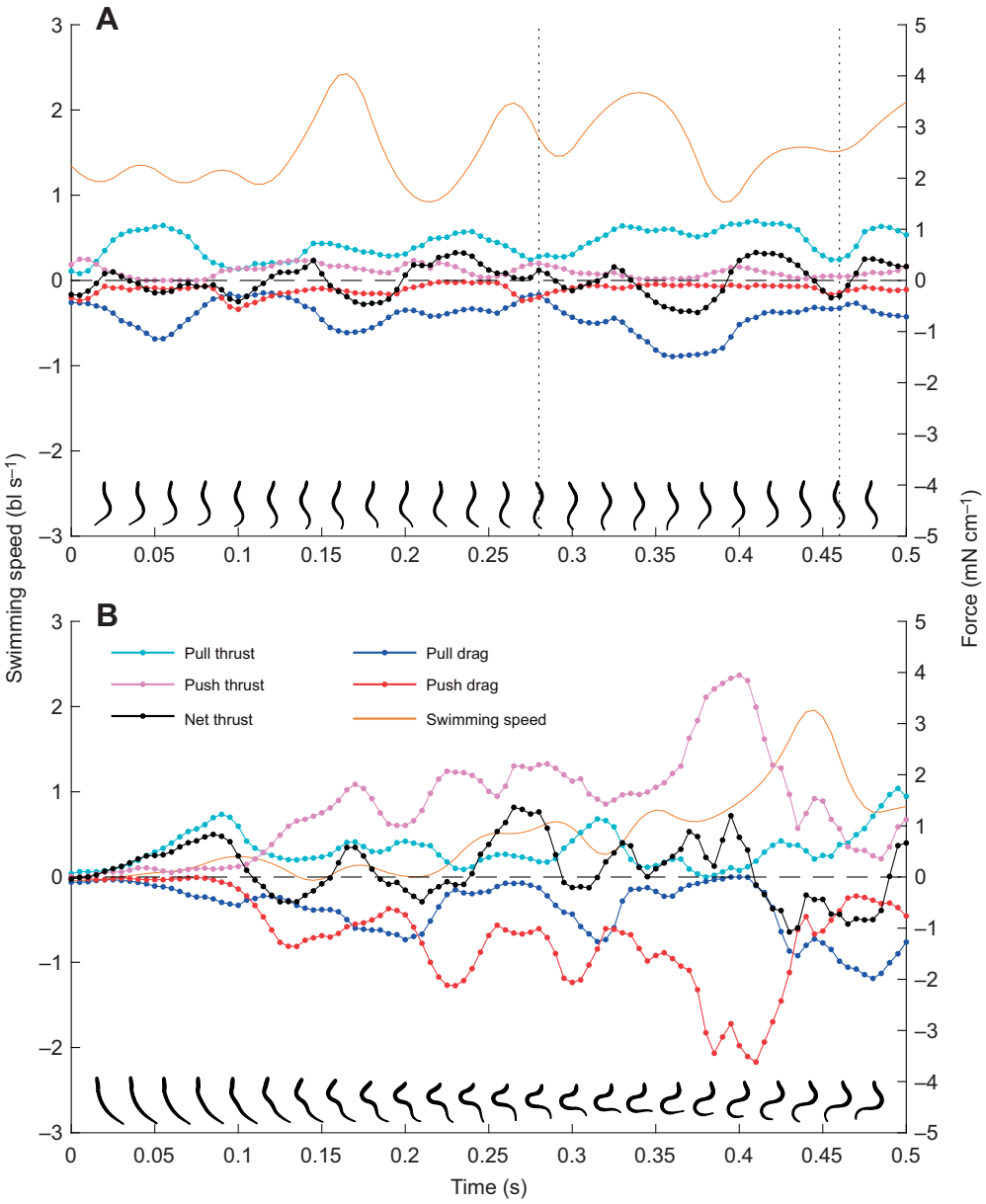

Fig. 6. Swimming speed and force components versus time. Swimming speed, total body thrust and drag components, and body outlines plotted against time for example sequences of (A) steady swimming and (B) acceleration from rest. In A, the dotted lines indicate boundaries between half-cycles. In B, one half-cycle is shown.

During late acceleration, the high-pressure region shifted toward the tail. The tail was orientated approximately perpendicular to the swimming direction (Fig. 4F,I), and positive pressure near the tail was the dominant contributor to thrust (Fig. 7D). Thrust shifted posteriorly compared with early acceleration, with the anterior, medial and posterior thirds of the body contributing 18.4%, 29.2% and 52.4% of thrust. At the end of the first half-cycle of acceleration from rest, thrust forces shifted from push-dominated thrust to pull-dominated thrust more typical of steady swimming (Fig. 6A).

DISCUSSION

Steady swimming

Previous studies of anguilliform swimming have debated the role of the body in thrust production. Some studies have found that the entire body contributes to thrust production (Carling et al., 1998; Videler et al., 1999; Müller et al., 2001; Chen et al., 2011; Gemmell et al., 2016), while others have emphasized the importance of the tail and minimized the importance of the rest of the body (Lighthill, 1971; Tytell and Lauder, 2004). During steady swimming, thrust and drag must balance and their effects cannot be separated in the wake (Schultz and Webb, 2002; Tytell, 2007). Detailed flow and force measurements along the length of the fish's body are thus needed to determine the relative roles of the body and tail in thrust production.

Müller et al. (2001) found that flow speed increased steadily from head to tail along the body of a steadily swimming European eel (*Anguilla anguilla*). They concluded that thrust was generated along the length of the body, which they explained based on the 'undulatory pump mechanism', in which flow is generated by low-pressure regions on the concave sides of body bends (Blickhan et al., 1992). Müller et al. (2001) proposed that high vorticity regions, known as 'proto-vortices' developed in this way travel along the body until they reach the tail, where they are shed as 'body' vortices, as opposed to 'tail' vortices generated by the trailing edge of the tail. In contrast, Tytell and Lauder (2004) in their study of American eels (*Anguilla rostrata*) de-emphasized the role of the body in thrust production. They found that velocity increased slowly along the front of the body and that vorticity of proto-vortices

Journal of Experimental Biology (2019) 222, jeb212464. doi:10.1242/jeb.212464

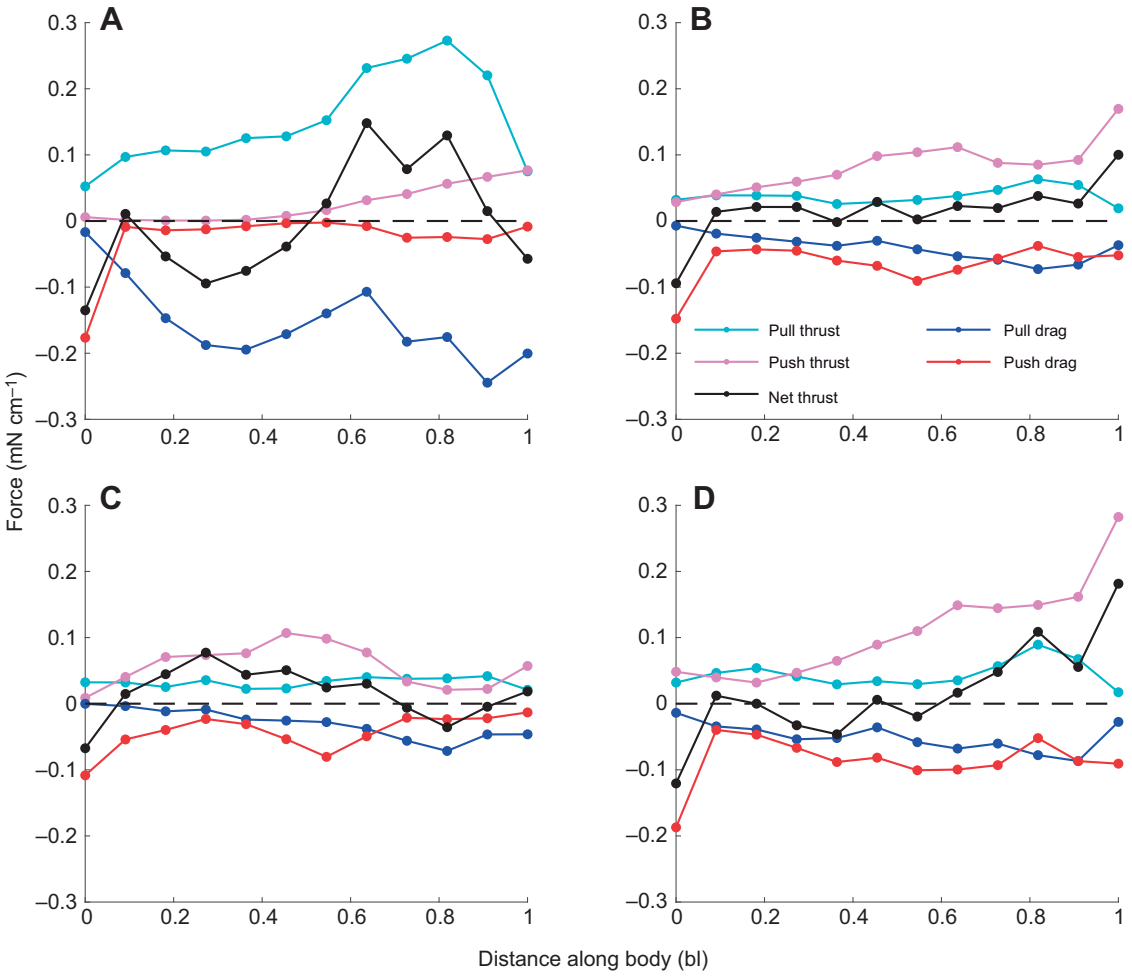

Fig. 7. Distribution of forces along the body. Mean force components plotted against normalized distance along the body, starting at the snout, averaged over (A) a half-cycle of steady swimming (n=8), (B) a half cycle of acceleration from rest (n=8), or the first (C) and second (D) halves (early and late, respectively) of the acceleration half cycle.

was low compared with that of tail vortices. Studies of a robotic swimmer designed to mimic lamprey kinematics also concluded that thrust is generated mainly near the tail (Hultmark et al., 2007; Leftwich and Smits, 2011).

We calculated forces acting on the body, allowing us to quantify the contribution of each section of the body to thrust and drag (Fig. 7). As previously demonstrated (Gemmell et al., 2015a, 2016), thrust was derived primarily from negative pressure during steady swimming (Figs 4D,G and 7A). We found that thrust increased gradually toward the posterior of the animal, with net thrust concentrated along the rear half of the body (Fig. 7). Based on these results, the entire body contributes to thrust in steady lamprey swimming, but thrust exceeds drag only over the rear half of the body. Our data thus help to reconcile seemingly contradictory results from previous studies.

Acceleration from rest

The demands of steady swimming and escape swimming differ substantially. For steady swimming, especially during long migrations (Beamish, 1980), low energy consumption is vital. For escape swimming, initiating swimming as soon as possible is of greater importance. The kinematics and hydrodynamics of acceleration from rest differed in several ways from those of steady swimming. The initial body waves produced by lampreys accelerating from rest were visibly larger and slower than those produced during steady swimming, with significantly greater mean amplitude and wavelength and significantly slower mean wave speed (Fig. 3). Whereas steady swimming was associated with predominately negative pressure (relative to ambient) and pull-derived thrust, acceleration from rest was associated with predominately positive pressure and push-derived thrust (Fig. 5). The kinematic and hydrodynamic differences between the two swimming modes suggest distinct mechanisms that may be adapted to the differing demands of steady swimming and escape swimming.

Lampreys had significantly slower body wave speed during acceleration from rest than during steady swimming (Fig. 3D). A study of *A. rostrata* swimming found that body wave speed and swimming speed were highly positively correlated (Tytell, 2004), so the difference in wave speed may have been a product of the faster swimming speed of the steady swimming sequences. Slip is defined as the ratio of swimming speed to wave speed. Slip values less than one are associated with acceleration, and slip values greater than one are associated with deceleration (Müller et al., 2002). Slip was significantly lower for accelerating swimming (0.23±0.07) than for steady swimming (0.62±0.05, P=0.0002), in line with the association between acceleration and low slip values. Despite an overall negative mean acceleration, however, slip was less than one for steady swimming.

During acceleration from rest, lampreys produced a high-amplitude body bend that most often formed approximately one-quarter body length posterior to the head. Tytell (2004) similarly noted that *A. rostrata* produced higher amplitude body waves during acceleration (not from rest) than steady swimming. The push force on the posterior side of this bend (Fig. 4E,H) initiated acceleration during the preparatory stroke of escape swimming, well before the formation of the first tail vortex (Fig. 6). The reliance of acceleration from rest on thrust from positive pressure provides a likely explanation for the distinctive body kinematics that characterize the initial preparatory stroke of escape swimming. The high-amplitude bend produces a high-pressure region along a large surface area opposite to the swimming direction, which directs much of the push force to useable thrust. While presenting a large surface area perpendicular to the swimming direction would increase drag considerably during steady swimming, its drag contribution during early acceleration appears to be modest (Figs 4H and 7C) as a result of the low swimming speed at this stage of acceleration from rest.

As the large pressure region posterior to the first body bend develops, a second, smaller push force develops at the head (Fig. 4E,H). To our knowledge, the importance of the head in thrust production during acceleration from rest has not previously been recognized, but a computational study of larval zebrafish swimming, which is considered a form of anguilliform locomotion (Müller et al., 2008), showed contralateral high- and low-pressure regions adjacent to the head at the beginning of acceleration, similar to those seen in our pressure fields (Fig. 4E; Li et al., 2012, their fig. 19).

The shift from push-dominated to pull-dominated thrust during the transition from acceleration from rest to steady swimming suggests that undulatory swimmers can generate push thrust at low speeds, whereas pull thrust develops at higher speeds. Transected lampreys that are unable to produce the strong negative pressure regions necessary for pull thrust have been shown to swim less efficiently than control lampreys (Gemmell et al., 2015a, 2016), but the negative pressure regions that lead to pull thrust are associated with vortices along the body that require time to develop. Thus, push thrust used during acceleration from rest may be faster to develop but less efficient than pull thrust, reflecting the different demands associated with acceleration from rest and steady swimming.

Conclusions

Time is critical during escape swimming, and the large push force generated by a deep initial body bend enables a lamprey to accelerate before the first body wave reaches its tail (Fig. 6B). Kinematics similar to the acceleration mechanism examined here could also be important in low-speed turning and maneuvering in which drag-based mechanisms are less effective.

Anguilliform undulatory swimmers have inspired the design of underwater vehicles that have been used to study aquatic locomotion (Melsaac and Ostrowski, 1999; Hultmark et al., 2007; Leftwich and Smits, 2011; Leftwich et al., 2012; Bale et al., 2014) and for underwater exploration, e.g. for hunting mines (Wilbur et al., 2002). These robots are generally designed based on the kinematics and hydrodynamics of steady swimming. Incorporating elements of unsteady swimming into swimming robot designs could improve the ability of these robots to accelerate and maneuver at low speeds.

Acknowledgements

We would like to thank Hailley Nieves for her assistance with experiments and two anonymous reviewers for their helpful comments.

Competing interests

The authors declare no competing or financial interests.

Author contributions

Conceptualization: K.T.D., J.O.D., J.H.C., S.P.C., J.R.M., S.M.F.; Methodology: K.T.D., J.O.D., J.H.C., S.P.C., B.J.G.; Software: K.T.D., J.O.D.; Validation: K.T.D.; Formal analysis: K.T.D.; Investigation: K.T.D.; Resources: J.R.M., S.M.F.; Writing - original draft: K.T.D.; Writing - review & editing: K.T.D., J.O.D., J.H.C., S.P.C., J.R.M., S.M.F., B.J.G.; Visualization: K.T.D.; Funding acquisition: B.J.G.

Funding

This research was supported by grants from the National Science Foundation (UNS-1511996 and IDBR-1455471 to B.J.G., J.O.D., S.P.C. and J.H.C.). J.R.M. was funded by the Marine Biological Laboratory.

Data availability

Videos of larval sea lampreys swimming steadily or accelerating from rest have been deposited in the figshare digital repository: 10.6084/m9.figshare.8284019.

References

Bale, R., Shirgaonkar, A. A., Neveln, I. D., Bhalla, A. P. S., MacIver, M. A. and Patankar, N. A. (2014). Separability of drag and thrust in undulatory animals and machines. *Sci. Rep.* **4**, 7329. doi:10.1038/srep07329

Beamish, F. W. H. (1980). Biology of the North American anadromous sea lamprey, *Petromyzon marinus*. *Can. J. Fish. Aquat. Sci.* **37**, 1924-1943. doi:10.1139/f80-233

Blickhan, R., Krick, C., Zehren, D., Nachtigall, W. and Breithaupt, T. (1992). Generation of a vortex chain in the wake of a suhundulatory swimmer. *Naturwissenschaften* **79**, 220-221. doi:10.1007/BF01227131

Carling, J., Williams, T. L. and Bowtell, G. (1998). Self-propelled anguilliform swimming: simultaneous solution of the two-dimensional Navier-Stokes equations and Newton's laws of motion. *J. Exp. Biol.* **201**, 3143-3166.

Chen, J., Friesen, W. O. and Iwasaki, T. (2011). Mechanisms underlying rhythmic locomotion: body–fluid interaction in undulatory swimming. *J. Exp. Biol.* **214**, 561-574. doi:10.1242/jeb.048751

Dabiri, J. O., Bose, S., Gemmell, B. J., Colin, S. P. and Costello, J. H. (2014). An algorithm to estimate unsteady and quasi-steady pressure fields from velocity field measurements. *J. Exp. Biol.* **217**, 331-336. doi:10.1242/jeb.092767

Domenici, P. and Blake, R. (1997). The kinematics and performance of fish fast-start swimming. *J. Exp. Biol.* **200**, 1165-1178.

Domenici, P. and Hale, M. E. (2019). Escape responses of fish: a review of the diversity in motor control, kinematics and behaviour. *J. Exp. Biol.* **222**, jeb166009. doi:10.1242/jeb.166009

Eaton, R. C., Lee, R. K. K. and Foreman, M. B. (2001). The mauthner cell and other identified neurons of the brainstem escape network of fish. *Prog. Neurobiol.* **63**, 467-485. doi:10.1016/S0301-0082(00)00047-2

Flammang, B. E., Lauder, G. V., Troolin, D. R. and Strand, T. (2011). Volumetric imaging of shark tail hydrodynamics reveals a three-dimensional dual-ring vortex wake structure. *Proc. R. Soc. B* **278**, 3670-3678. doi:10.1098/rspb.2011.0489

Gazzola, M., Van Rees, W. M. and Koumoutsakos, P. (2012). C-start: optimal start of larval fish. *J. Fluid Mech.* **698**, 5-18. doi:10.1017/jfm.2011.558

Gemmell, B. J., Adhikari, D. and Longmire, E. K. (2014). Volumetric quantification of fluid flow reveals fish's use of hydrodynamic stealth to capture evasive prey. *J. R. Soc. Interface* **11**, 20130880. doi:10.1098/rsif.2013.0880

Gemmell, B. J., Colin, S. P., Costello, J. H. and Dabiri, J. O. (2015a). Suction-based propulsion as a basis for efficient animal swimming. *Nat. Commun.* **6**, 8790. doi:10.1038/ncomms9790

Gemmell, B. J., Troolin, D. R., Costello, J. H., Colin, S. P. and Satterlie, R. A. (2015b). Control of vortex rings for manoeuvrability. *J. R. Soc. Interface* **12**, 20150389. doi:10.1098/rsif.2015.0389

Gemmell, B. J., Fogerson, S. M., Costello, J. H., Morgan, J. R., Dabiri, J. O. and Colin, S. P. (2016). How the bending kinematics of swimming lampreys build negative pressure fields for suction thrust. *J. Exp. Biol.* **219**, 3884-3895. doi:10.1242/jeb.144642

Gillis, G. B. (1996). Undulatory locomotion in elongate aquatic vertebrates: anguilliform swimming since sir james gray. *Am. Zool.* **36**, 656-665. doi:10.1093/icb/36.6.656

Gray, J. (1933). Studies in animal locomotion. *J. Exp. Biol.* **10**, 88-104.

Gurka, R., Liberzon, A., Hefetz, D., Rubinstein, D. and Shavit, U. (1999). Computation of pressure distribution using piv velocity data. In *Proceedings of the 3rd International Workshop on Particle Image Velocimetry*, Vol. 2 (ed. R. Adrian), pp. 671-676. Berlin: Springer.

Hultmark, M., Leftwich, M. and Smits, A. J. (2007). Flowfield measurements in the wake of a robotic lamprey. *Exp. Fluids* **43**, 683-690. doi:10.1007/s00348-007-0412-1

Kurt, M., Cochran-Carney, J., Zhong, Q., Mivehchi, A., Quinn, D. B. and Moored, K. W. (2019). Swimming freely near the ground leads to flow-mediated equilibrium altitudes. *J. Fluid Mech.* **875**. doi:10.1017/jfm.2019.540

Lauder, G. V. (2015). Fish locomotion: recent advances and new directions. *Annu. Rev. Mar. Sci.* **7**, 521-545. doi:10.1146/annurev-marine-010814-015614
Lauder, G. V. and Tytell, E. D. (2005). Hydrodynamics of undulatory propulsion. *Fish Physiol.* **23**, 425-468. doi:10.1016/S1546-5098(05)23011-X
Leftwich, M. C. and Smits, A. J. (2011). Thrust production by a mechanical swimming lamprey. *Exp. Fluids* **50**, 1349-1355. doi:10.1007/s00348-010-0994-x
Leftwich, M. C., Tytell, E. D., Cohen, A. H. and Smits, A. J. (2012). Wake structures behind a swimming robotic lamprey with a passively flexible tail. *J. Exp. Biol.* **215**, 416-425. doi:10.1242/jeb.061440
Li, G., Müller, U. K., van Leeuwen, J. L. and Liu, H. (2012). Body dynamics and hydrodynamics of swimming fish larvae: a computational study. *J. Exp. Biol.* **215**, 4015-4033. doi:10.1242/jeb.071837
Li, G., Müller, U. K., van Leeuwen, J. L. and Liu, H. (2014). Escape trajectories are deflected when fish larvae intercept their own c-start wake. *J. R. Soc. Interface* **11**, 20140848. doi:10.1098/rsif.2014.0848
Lighthill, M. (1971). Large-amplitude elongated-body theory of fish locomotion. *Proc. R. Soc. B* **179**, 125-138. doi:10.1098/rspb.1971.0085
Linden, P. F. and Turner, J. S. (2004). 'Optimal' vortex rings and aquatic propulsion mechanisms. *Proc. R. Soc. B* **271**, 647-653. doi:10.1098/rspb.2003.2601
Lucas, K. N., Dabiri, J. O. and Lauder, G. V. (2017). A pressure-based force and torque prediction technique for the study of fish-like swimming. *PLoS ONE* **12**, e0189225. doi:10.1371/journal.pone.0189225
Melsaac, K. and Ostrowski, J. P. (1999). A geometric approach to anguilliform locomotion: modelling of an underwater eel robot. In IEEE International Conference on Robotics and Automation, Vol. 4, pp. 2843-2848. New York: IEEE. doi:10.1109/robot.1999.774028
Müller, U., Van Den Heuvel, B., Stamhuis, E. and Videler, J. (1997). Fish foot prints: morphology and energetics of the wake behind a continuously swimming mullet (chelon labrosus risso). *J. Exp. Biol.* **200**, 2893-2906.
Müller, U. K., Smit, J., Stamhuis, E. J. and Videler, J. J. (2001). How the body contributes to the wake in undulatory fish swimming. *J. Exp. Biol.* **204**, 2751-2762.
Müller, U. K., Stamhuis, E. J. and Videler, J. J. (2002). Riding the waves: the role of the body wave in undulatory fish swimming. *Integr. Comp. Biol.* **42**, 981-987. doi:10.1093/icb/42.5.981
Müller, U. K., van den Boogaart, J. G. and van Leeuwen, J. L. (2008). Flow patterns of larval fish: undulatory swimming in the intermediate flow regime. *J. Exp. Biol.* **211**, 196-205. doi:10.1242/jeb.005629
Nair, A., Azatian, G. and McHenry, M. J. (2015). The kinematics of directional control in the fast start of zebrafish larvae. *J. Exp. Biol.* **218**, 3996-4004. doi:10.1242/jeb.126292
Noca, F., Shiels, D. and Jeon, D. (1997). Measuring instantaneous fluid dynamic forces on bodies, using only velocity fields and their derivatives. *J. Fluid Struct.* **11**, 345-350. doi:10.1006/jfls.1997.0081
Noca, F., Shiels, D. and Jeon, D. (1999). A comparison of methods for evaluating time-dependent fluid dynamic forces on bodies, using only velocity fields and their derivatives. *J. Fluid Struct.* **13**, 551-578. doi:10.1006/jfls.1999.0219
Schultz, W. W. and Webb, P. W. (2002). Power requirements of swimming: do new methods resolve old questions? *Integr. Comp. Biol.* **42**, 1018-1025. doi:10.1093/icb/42.5.1018
Tytell, E. D. (2004). Kinematics and hydrodynamics of linear acceleration in eels, *Anguilla rostrata*. *Proc. R. Soc. B* **271**, 2535-2540. doi:10.1098/rspb.2004.2901
Tytell, E. D. (2007). Do trout swim better than eels? challenges for estimating performance based on the wake of self-propelled bodies. *Exp. Fluids* **43**, 701-712. doi:10.1007/s00348-007-0343-x
Tytell, E. D. and Lauder, G. V. (2004). The hydrodynamics of eel swimming: I. Wake structure. *J. Exp. Biol.* **207**, 1825-1841. doi:10.1242/jeb.00968
Tytell, E. D. and Lauder, G. V. (2008). Hydrodynamics of the escape response in bluegill sunfish, *Lepomis macrochirus*. *J. Exp. Biol.* **211**, 3359-3369. doi:10.1242/jeb.020917
van Oudheusden, B. W., Scarano, F., Roosenboom, E. W. M., Casimiri, E. W. F. and Souverein, L. J. (2007). Evaluation of integral forces and pressure fields from planar velocimetry data for incompressible and compressible flows. *Exp. Fluids* **43**, 153-162. doi:10.1007/s00348-007-0261-y
Videler, J., Muller, U. and Stamhuis, E. (1999). Aquatic vertebrate locomotion: wakes from body waves. *J. Exp. Biol.* **202**, 3423-3430.
Wakeling, J. M. (2005). Fast-start mechanics. *Fish Physiol.* **23**, 333-368. doi:10.1016/S1546-5098(05)23009-1
Wald, G. (1957). The metamorphosis of visual systems in the sea lamprey. *J. Gen. Physiol.* **40**, 901-914. doi:10.1085/jgp.40.6.901
Webb, P. W. (2002). Kinematics of plaice, pleuronectes platessa, and cod, gadus morhua, swimming near the bottom. *J. Exp. Biol.* **205**, 2125-2134.
Wilbur, C., Vorus, W. and Cao, Y. (2002). A lamprey-based undulatory vehicle. In *Neurotechnology for Biomimetic Robots* (ed. J. Ayers, J. L. Davis and A. Rudolph), pp. 285-296. MIT Press.